SUPPLEMENTARY INFORMATION

SUPPLEMENTARY NOTES

Supplementary Note 1: Common strategies against the battery problem

The strategies to overcome the battery problem mainly narrow down to two main methods: ambient energy harvesting and wireless power transfer[1]. Among these methods, wireless power transfer schemes could offer greater power densities, with near field inductive coupling scheme at the forefront[2,3]. Based on this inductive coupling, near-field communication (NFC) technology have already been utilized in various healthcare applications[4], including wearable pulse oximetry, EEG, PPG, pressure & temperature sensing[5–7] to implantable optoelectronic systems for neuroscience[8–10] and soft contact lenses for IOP and tear-based biomarker sensing[11–13]. However, NFC-based technologies require application-specific integrated circuits, which limit their use to that specific application and hinder design freedom to general use[14]. On the other hand, well-established inductive-coupling based sensing approaches eliminate the need for ASICs by utilizing passive resonant sensors and offer great design flexibility, as demonstrated by numerous applications[15–17]. Besides, inductively coupled approaches are reported for transducers for various applications as well[18,19]. Nevertheless, for emerging technologies like wearable ultrasound, such battery-free operation schemes have not been demonstrated.

Supplementary Note 2: Blood pressure waveform calculation

Ultrasonic time-of-flight measurement-based blood pressure calculation is achieved by the measurement of the artery diameter as described in[20ï 25]. More specifically, to accurately calculate blood pressure using carotid artery measurements, we first determine the artery diameter based on time-of-flight (TOF) assessments for the anterior and posterior arterial walls. The TOF measurements, derived from region-of-interest (ROI) bands generated during a calibration workflow, capture the dynamic echo movements of these walls. Initially, the artery diameter is computed from the TOF values of the anterior and posterior walls in the calibration workflow. The difference in TOF between the posterior and anterior walls, known as g TOF, represents the arterial oscillation during each cardiac cycle. The total TOF is obtained by summing the TOF for each arterial wall with g TOF, yielding a complete time value that serves as the basis for diameter calculation. Given that ultrasound signals traverse and then reflect from the arterial walls, the TOF effectively measures twice the diameter. Therefore, the artery diameter is derived by dividing the product of tissue speed of sound and TOF by two. Using the calculated artery diameter $d(t)$, the cross-sectional area of the carotid artery, denoted A(t), is computed as:

$$A(t) = \frac{\pi d^2(t)}{4}$$

The maximum and minimum values of A(t) correspond to the systolic A_s and diastolic A_d artery areas, respectively. To determine the alpha coefficient α, which is essential for calculating blood pressure, the following relation is used:

$$and\ \alpha = \frac{A_d * \ln\left(\frac{p_s}{p_d}\right)}{A_s - A_d}$$

where p_s and p_d represent the systolic and diastolic blood pressures, respectively. Finally, we compute blood pressure by:

$$p(t) = p_d + e^{\alpha\left(\frac{A(t)}{A_d} - 1\right)}$$

Here, the term $A(t)/A_d$ ī 1 accounts for the arterial expansion relative to the diastolic baseline, scaled by α, and is added to p_d to obtain the real-time blood pressure values.

SUPPLEMENTARY FIGURES

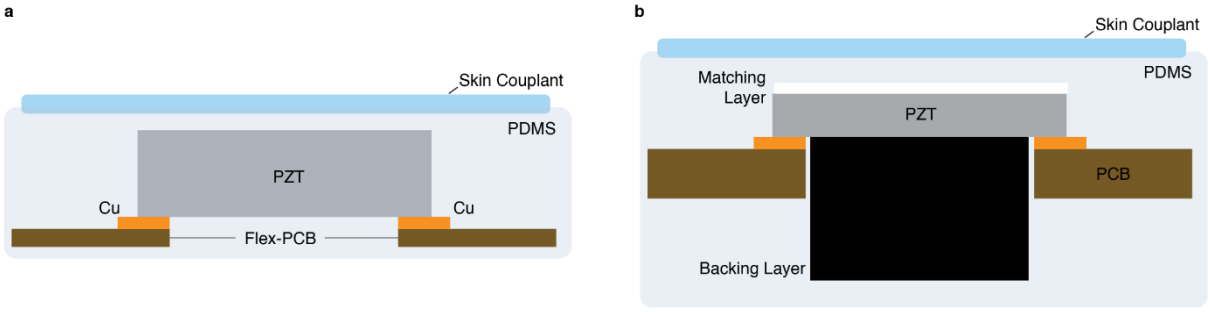

Supplementary Fig. 1. Schematic cross-sectional view of the US tags.
Depending on the application requirements, tags can be designed with a coil on a flex-pcb and without matching layer (a) or on a rigid PCB with conventional matching and backing layers (b) to improve the bandwidth.

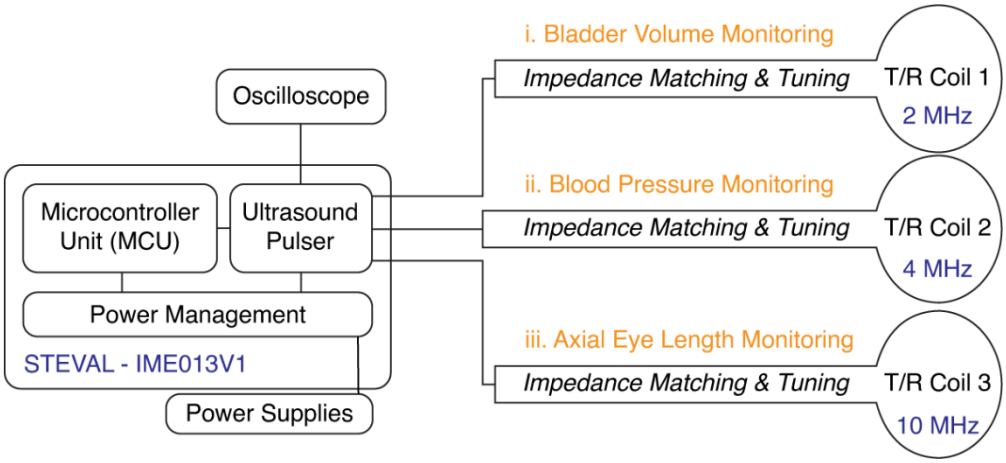

Supplementary Fig. 2. Simplified block diagram of a portable interrogator.
By utilizing off-the-shelf components, the US tags can be simply interrogated with pre-programmed microcontrollers, pulser ICs and T/R coils.

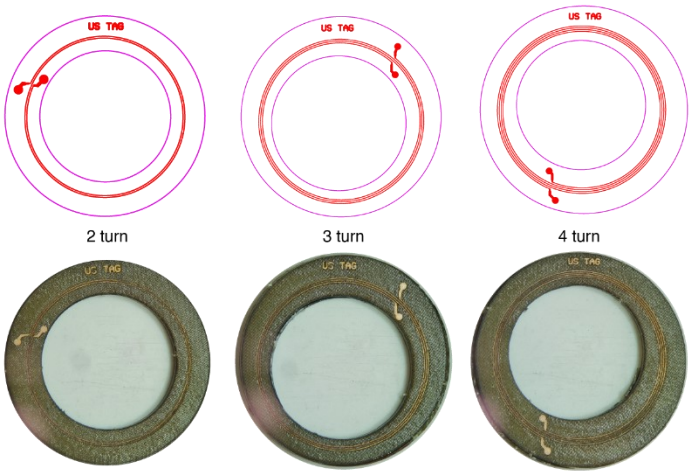

Supplementary Fig. 3. Representative transducer coil optimization for blood pressure monitoring.
By estimating an inductance value, coils with identical radii were designed with varying turn numbers. Designed coils were fabricated on standard FR4 PCBs. After soldering the coils to the ultrasonic transducer, S11 measurements revealed the top performing coil.

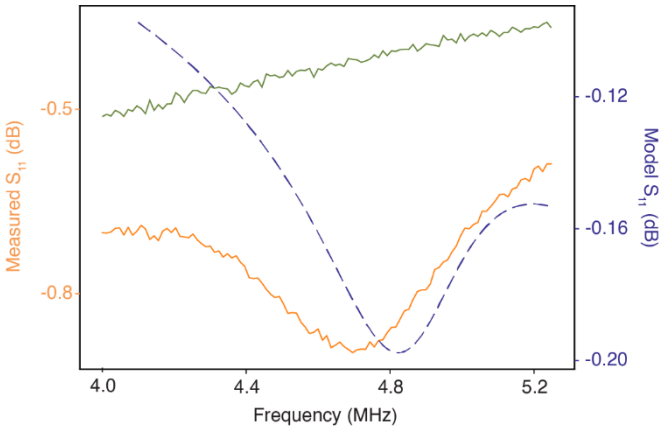

Supplementary Fig. 4. Expected and measured S11 of reader coil with and without blood pressure monitoring US tag nearby.

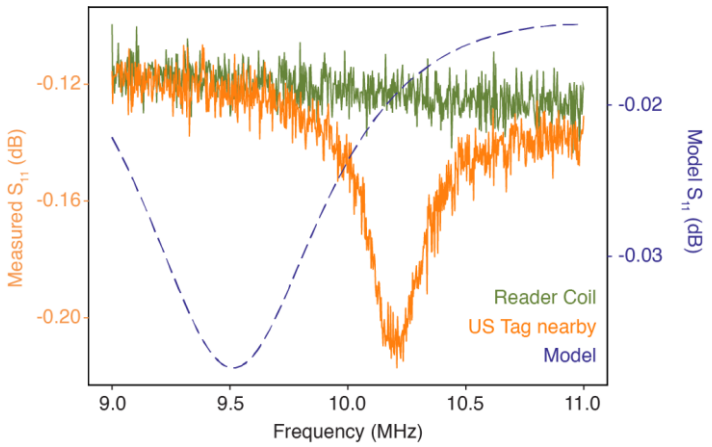

Supplementary Fig. 5. Expected and measured S11 of the reader coil with and without axial eye length monitoring US tag nearby.

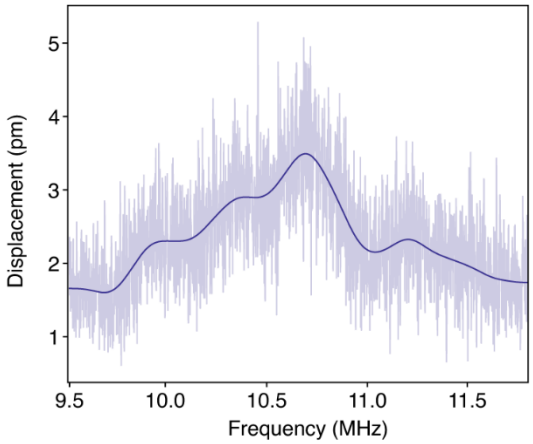

Supplementary Fig. 6. Laser Doppler Vibrometry measurements of the wirelessly excited axial eye length monitoring US tag.

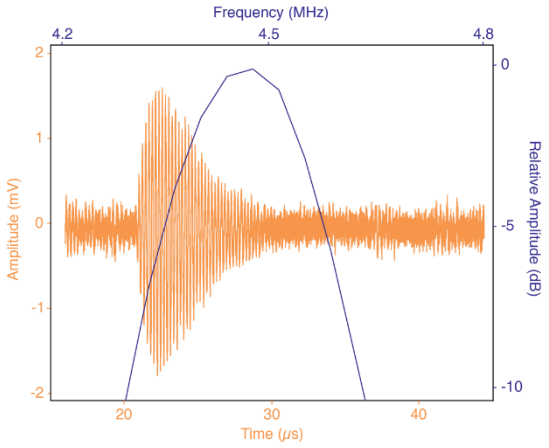

Supplementary Fig. 7. Pulse-echo response and derived frequency spectra of the wirelessly excited blood pressure monitoring US tag.

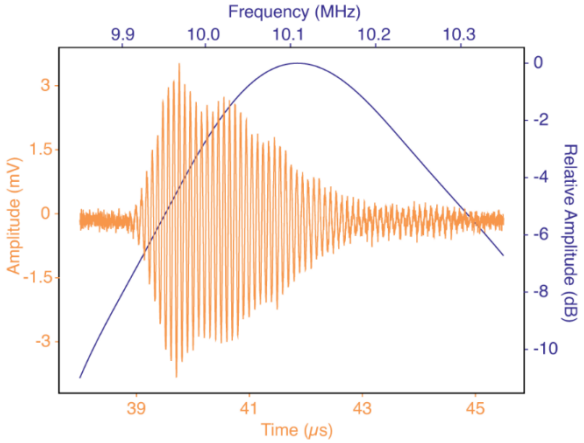

Supplementary Fig. 8. Pulse-echo response and derived frequency spectra of the wirelessly excited axial eye length monitoring US tag.

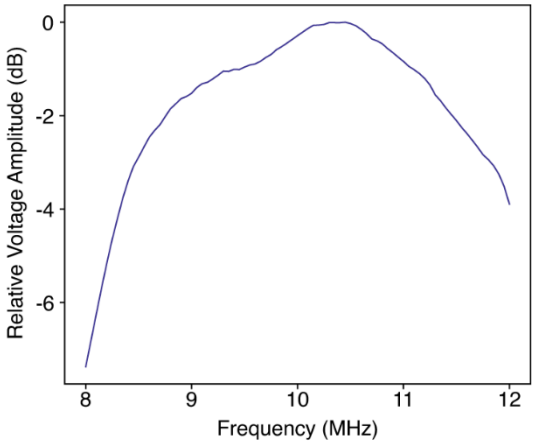

Supplementary Fig. 9. Underwater frequency sweep of the wirelessly excited axial eye length monitoring US tag captured by a hydrophone.

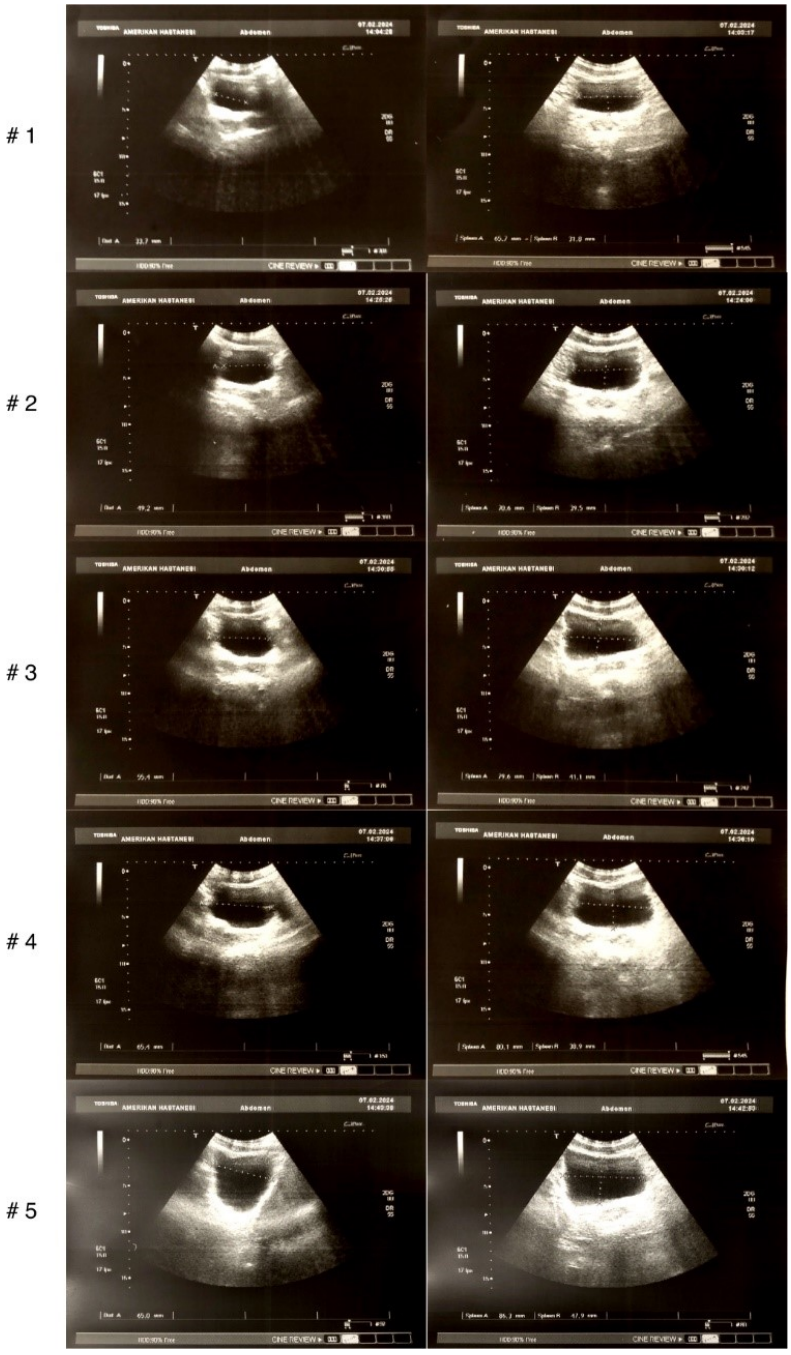

Supplementary Fig. 10. Bladder ultrasound images of the volunteer (1-5).

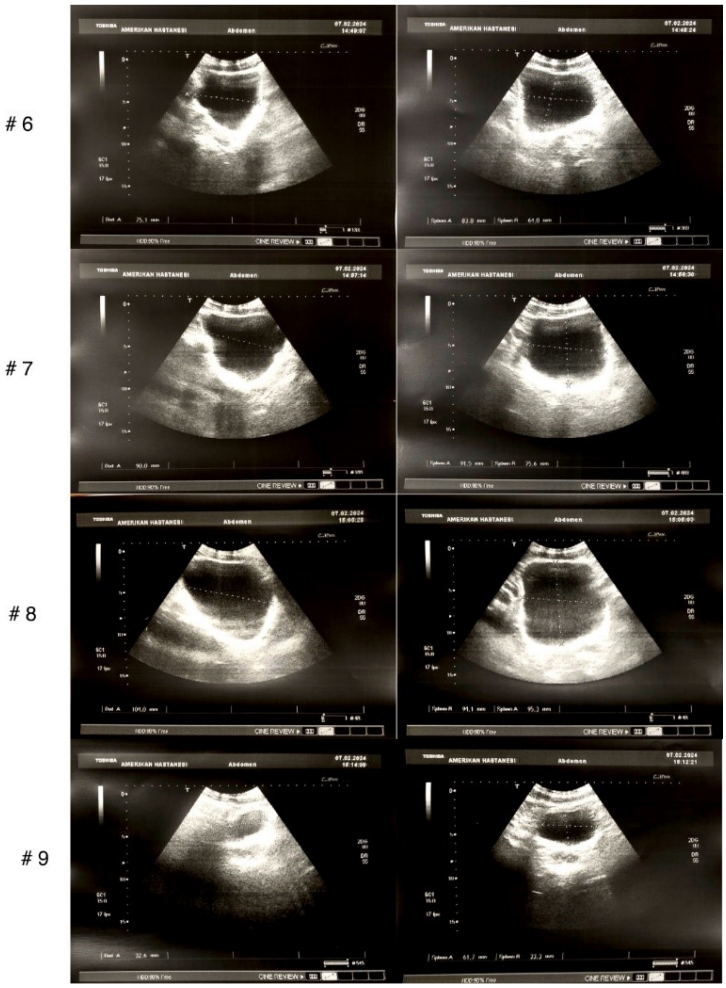

Supplementary Fig. 11. Bladder ultrasound images of the volunteer (6-9).

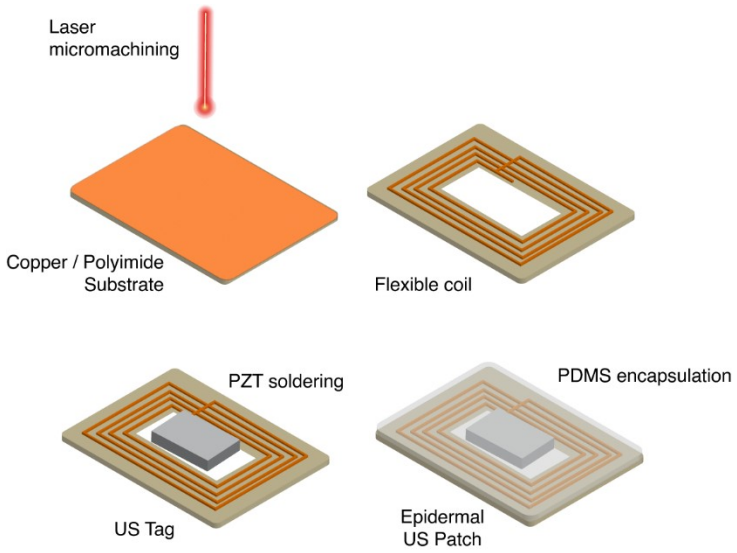

Supplementary Fig. 12. Fabrication flow of US tag in epidermal US patch format. For applications with less strict requirements on bandwidth, use of additional layers can be avoided.

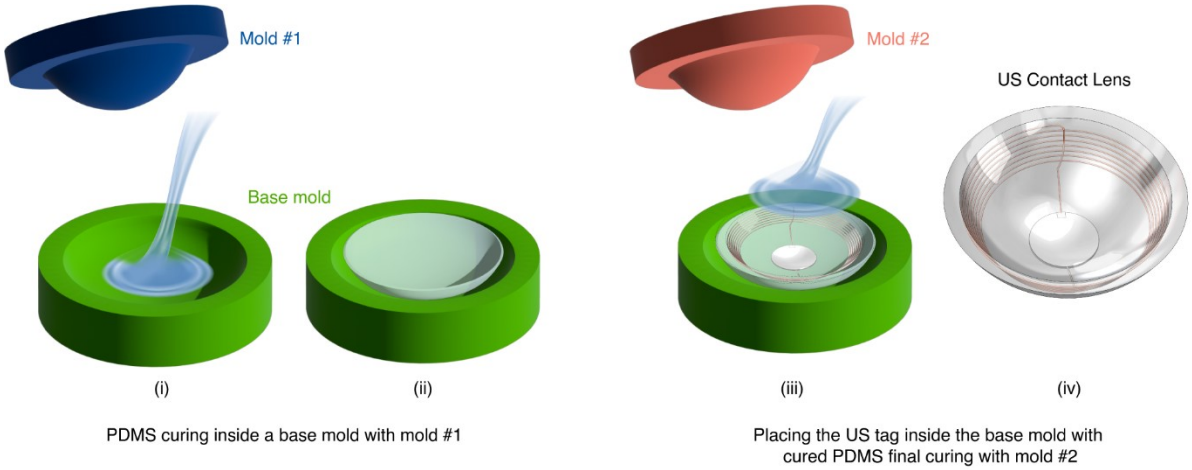

Supplementary Fig. 13. Fabrication flow of US tag in US contact lens.

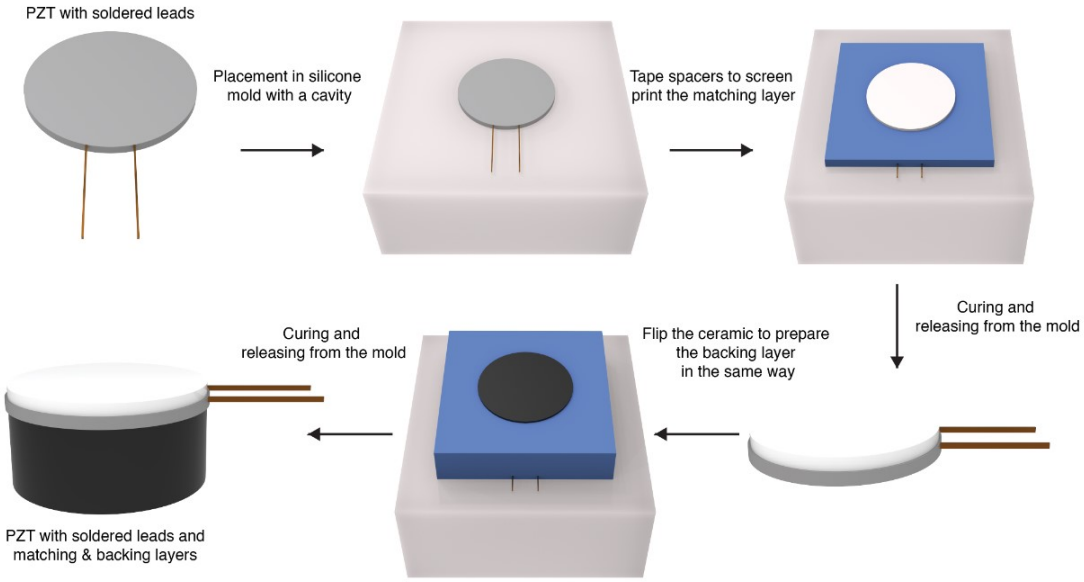

Supplementary Fig. 14. Fabrication flow of US tag in epidermal US patch format with matching and backing layers.
For applications with strict bandwidth requirements, matching and backing layers can be used for improved performance.

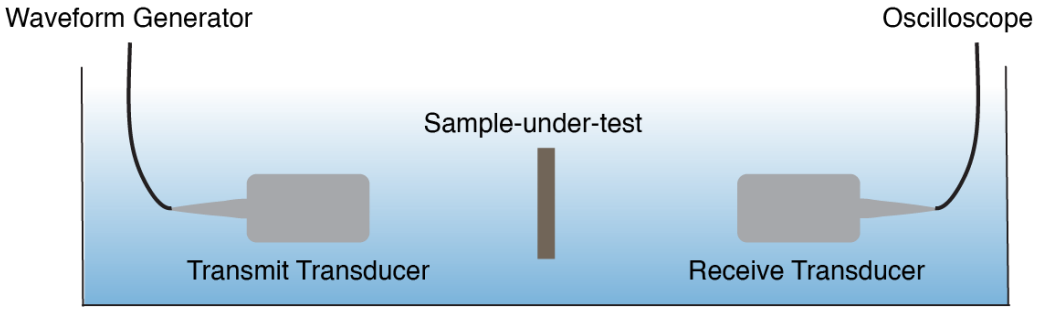

Supplementary Fig. 15. Material speed of sound & attenuation measurement setup for the characterization of matching and backing layers.
Two identical transducers were used as a transmitter and receiver couple. Measurements were taken with and without the sample-under-test in between the transducers. Alumina and tungsten loaded epoxy were used as the matching and backing layer. Based on five measurements, speed of sound of the matching layer was 2763 Ñ 26 m/s, and 918 Ñ 17 m/s for the backing layer. Attenuation coefficient values were 25 Ñ 1 dB/cm for the matching layer and 101 Ñ 14 dB/cm for the backing layer.

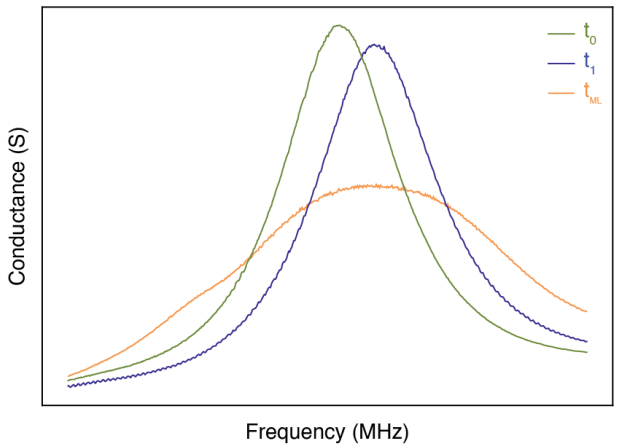

Supplementary Fig. 16. Conductance measurements of the transducer with matching and backing layers.
As the thickness approaches the required matching layer thickness, a broader response is observed.

References

1. Cheng, P. *et al.* An intrinsically stretchable power-source system for bioelectronics. *Device* **2**, (2024).
2. Nair, V. *et al.* Miniature battery-free bioelectronics. *Science (1979)* **382**, eabn4732 (2024).
3. Won, S. M., Cai, L., Gutruf, P. & Rogers, J. A. Wireless and battery-free technologies for neuroengineering. *Nat Biomed Eng* **7**, 405–423 (2023).
4. Olenik, S., Lee, H. S. & Güder, F. The future of near-field communication-based wireless sensing. *Nat Rev Mater* **6**, 286–288 (2021).
5. Kim, J. *et al.* Miniaturized Battery-Free Wireless Systems for Wearable Pulse Oximetry. *Adv Funct Mater* **27**, 1604373 (2017).
6. Chung, H. U. *et al.* Binodal, wireless epidermal electronic systems with in-sensor analytics for neonatal intensive care. *Science (1979)* **363**, eaau0780 (2019).
7. Han, H. *et al.* Battery-Free, Wireless, Ionic Liquid Sensor Arrays to Monitor Pressure and Temperature of Patients in Bed and Wheelchair. *Small* **19**, 2205048 (2023).
8. Kim, J. *et al.* Battery-free, stretchable optoelectronic systems for wireless optical characterization of the skin. *Sci Adv* **2**, e1600418 (2024).
9. Shin, G. *et al.* Flexible Near-Field Wireless Optoelectronics as Subdermal Implants for Broad Applications in Optogenetics. *Neuron* **93**, 509-521.e3 (2017).
10. Zhang, Y. *et al.* Battery-free, fully implantable optofluidic cuff system for wireless optogenetic and pharmacological neuromodulation of peripheral nerves. *Sci Adv* **5**, eaaw5296 (2024).
11. Kim, J. *et al.* A soft and transparent contact lens for the wireless quantitative monitoring of intraocular pressure. *Nat Biomed Eng* **5**, 772–782 (2021).
12. Mirzajani, H. *et al.* Femtosecond Laser Ablation Assisted NFC Antenna Fabrication for Smart Contact Lenses. *Adv Mater Technol* **7**, 2101629 (2022).
13. Ku, M. *et al.* Smart, soft contact lens for wireless immunosensing of cortisol. *Sci Adv* **6**, eabb2891 (2024).
14. Gutruf, P. *et al.* Fully implantable optoelectronic systems for battery-free, multimodal operation in neuroscience research. *Nat Electron* **1**, 652–660 (2018).
15. Chen, L. Y. *et al.* Continuous wireless pressure monitoring and mapping with ultra-small passive sensors for health monitoring and critical care. *Nat Commun* **5**, 5028 (2014).
16. Boutry, C. M. *et al.* Biodegradable and flexible arterial-pulse sensor for the wireless monitoring of blood flow. *Nat Biomed Eng* **3**, 47–57 (2019).
17. Carr, A. R. *et al.* Sweat monitoring beneath garments using passive, wireless resonant sensors interfaced with laser-ablated microfluidics. *NPJ Digit Med* **3**, 62 (2020).
18. Zhong, C. H., Croxford, A. J. & Wilcox, P. D. Investigation of inductively coupled ultrasonic transducer system for NDE. *IEEE Trans Ultrason Ferroelectr Freq Control* **60**, 1115–1125 (2013).
19. Badilita, V. *et al.* Microfabricated Inserts for Magic Angle Coil Spinning (MACS) Wireless NMR Spectroscopy. *PLoS One* **7**, e42848- (2012).
20. Peng, C., Chen, M., Sim, H. K., Zhu, Y. & Jiang, X. A Flexible Piezo-Composite Ultrasound Blood Pressure Sensor with Silver Nanowire-based Stretchable Electrodes. in *2020 IEEE 15th International Conference on Nano/Micro Engineered and Molecular System (NEMS)* 143–146 (2020). doi:10.1109/NEMS50311.2020.9265560.
21. Sempionatto, J. R. *et al.* An epidermal patch for the simultaneous monitoring of haemodynamic and metabolic biomarkers. *Nat Biomed Eng* **5**, 737–748 (2021).
22. Li, B. *et al.* Fabric-Based Ultrasonic Sensor with Integrated Piezoelectric Composite for Blood Pressure Monitoring. *Adv Mater Technol* **8**, 2201814 (2023).
23. Zhou, J. *et al.* Continuous and Non-Invasive Monitoring of Blood Pressure Based on Wearable Piezoelectric Micromachined Ultrasonic Transducers Array. *Journal of Microelectromechanical Systems* **32**, 437–444 (2023).

24. Sempionatto, J. R. *et al.* An epidermal patch for the simultaneous monitoring of haemodynamic and metabolic biomarkers. *Nature Biomedical Engineering 2021 5:7* **5**, 737–748 (2021).
25. Wang, C. *et al.* Monitoring of the central blood pressure waveform via a conformal ultrasonic device. *Nat Biomed Eng* **2**, 687–695 (2018).
26. Pomella, N., Rakobowchuk, M., Kolyva, C. & Khir, A. W. Changes in non-invasive wave intensity parameters with variations of Savitzky-Golay filter settings. in *2016 Computing in Cardiology Conference (CinC)* 1041–1044 (2016).